INTERNATIONAL JOURNAL OF EXPLORING EMERGING TRENDS IN ENGINEERING
Peer-Reviewed, Refereed, Indexed and International Journal, https://ijoeete.com/
(Peer Review Journal as per UGC 2025 Standard Guidelines)
|ISSN No. 2394-0573 |Volume: 13, Issue: 2 | April – June 2026

EFFECTS OF VARIABLE THICKNESS AND MELTING HEAT TRANSFER ON MHD NANOFLUID FLOW PAST A SLENDER STRETCHING SHEET

Preeti[1], Uma Shanker[2]

Department of Mathematics, Sunrise University, Alwar (Raj.), India

Email: [1]preeti598151@gmail.com, [2]yadav.umashanker@gmail.com

Abstract

This study investigates how variable sheet thickness combined with melting heat transfer influences the magnetohydrodynamic flow of an Ag–water nanofluid along a slender stretching surface. Similarity transformations convert the governing boundary-layer equations into a set of ordinary differential equations, which are then solved numerically using a shooting method paired with the classical fourth-order Runge–Kutta scheme. The impact of key parameters on velocity and temperature distributions, skin-friction coefficient and local Nusselt number is examined through graphs and tables. The numerical results show good agreement with earlier published data, confirming the reliability of the computational approach.

Keywords: Ag–water nanofluid; Melting heat transfer; Magnetohydrodynamics; Slender stretching sheet; Variable thickness

Introduction

Boundary-layer flows generated by stretching surfaces continue to attract significant attention because of their importance in polymer processing, glass-fibre production and continuous casting operations. Although most classical studies have considered sheets of uniform thickness, many industrial situations involve surfaces whose thickness changes gradually in the streamwise direction. Such variable-thickness (or slender) sheets appear when material is drawn under tension, and the resulting geometry strongly affects both the momentum and thermal boundary layers.

Several researchers have examined flows over slender stretching sheets. Babu et al.[1] studied convective heat transfer with temperature-dependent viscosity and viscous dissipation. Hayat et al.[2] analysed radiative flow over a rotating disk of variable thickness, while Asghar[3] investigated MHD nanofluid flow past a stretching surface. Kumar and Varma[4] included slip, chemical reaction and thermal radiation for a nanofluid over a permeable slender sheet. Mabood and Das[5] considered melting heat transfer together with second-order slip. Later works by Prasanna Kumara et al.[6], Fang et al.[7], Elbashbeshy et al.[8] and Abdel-wahed et al.[9] further clarified the roles of power-law stretching, thermal radiation and heat generation.

Acharya et al.[10] examined TiO_2– and Ag–water nanofluids over a slender sheet and noted that an increase in the thickness parameter lowers both fluid temperature and wall heat-transfer rate. Khan et al.[11] studied melting effects in Falkner–Skan flows of Carreau nanofluids, and Prasad et al.[12] investigated variable fluid properties under a transverse magnetic field. Additional contributions dealing with velocity slip, cross-diffusion, stagnation-point flow and nonlinear radiation have been reported by Babu and Sandeep[13], Hayat et al.[14,16], Gireesha et al.[15] and Qayyum et al.[17].

A series of papers by Anjali Devi and Prakash[18–20] treated hydromagnetic slip flow, temperature-dependent transport properties and thermal radiation over slender sheets. More recent contributions by Nadeem et al.[21,22], Parida and Mishra[23], Mishra and Das[24], Wakit et al.[25] and Rout and Mishra[26] have extended the analysis to chemical reactions, porous media and thermo-hydrodynamic stability of nanofluids.

Despite the large body of existing work, the combined influence of variable sheet thickness and melting heat transfer on the MHD flow of an Ag–water nanofluid has received relatively little attention. The present paper addresses this gap. The governing partial differential equations are reduced to ordinary differential equations by means of suitable

INTERNATIONAL JOURNAL OF EXPLORING EMERGING TRENDS IN ENGINEERING
Peer-Reviewed, Refereed, Indexed and International Journal, https://ijoeete.com/
(Peer Review Journal as per UGC 2025 Standard Guidelines)
|ISSN No. 2394-0573 |Volume: 13, Issue: 2 | April – June 2026

similarity transformations and are solved numerically by a shooting technique combined with the fourth-order Runge–Kutta method. The effects of the principal dimensionless parameters on velocity, temperature, skin friction and Nusselt number are discussed in detail.

Materials and Methods

Formulation of the Model

Consider the steady, two-dimensional, laminar flow of an electrically conducting, incompressible Ag–water nanofluid over an impermeable stretching sheet of variable thickness. The sheet occupies the region $y = A(x + b)^{(1-m)/2}$, where the constant A is sufficiently small that the pressure gradient across the sheet may be neglected ($\partial p/\partial x = 0$). The flow is driven by the continuous stretching of the sheet with velocity $U_w(x) = U_0(x + b)^m$, in which U_0 is a positive constant, b is a characteristic length and m is the power-law index. The analysis is restricted to $m \neq 1$; the special case $m = 1$ recovers the classical flat-sheet problem. A variable magnetic field of the form $B(x) = B_0(x + b)^{(m-1)/2}$ is applied transversely to the sheet surface. The wall and free-stream temperatures are denoted by T_m and T_∞, respectively, with $T_\infty > T_m$. Heat transfer at the solid–liquid interface is assumed to occur solely through melting. Viscous dissipation, Joule heating, thermal radiation and induced magnetic effects are neglected under the low magnetic Reynolds number approximation. The thermophysical properties of water and silver are listed in Table 1.

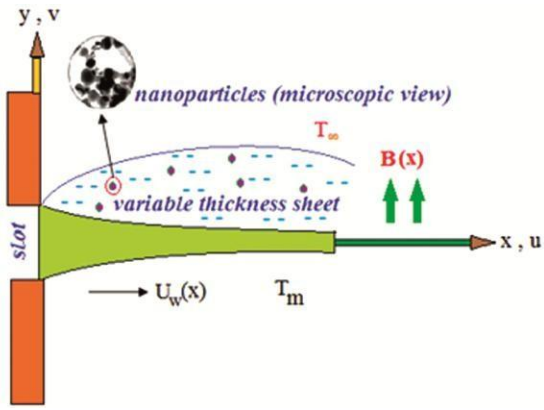

[Figure 1 — Physical model of the problem]

Under the foregoing assumptions the boundary-layer equations expressing conservation of mass, momentum and energy read

$$\frac{\partial u}{\partial x} + \frac{\partial v}{\partial y} = 0 \tag{1}$$

$$\rho_{nf}\left(u\frac{\partial u}{\partial x} + v\frac{\partial u}{\partial y}\right) = \mu_{nf}\frac{\partial^2 u}{\partial y^2} - \sigma_{nf}B^2(x)u \tag{2}$$

$$(\rho C_p)_{nf}\left(u\frac{\partial T}{\partial x} + v\frac{\partial T}{\partial y}\right) = \kappa_{nf}\frac{\partial^2 T}{\partial y^2} \tag{3}$$

Here u and v are the velocity components in the x- and y-directions, while ρ_{nf}, μ_{nf}, σ_{nf}, $(\rho C_p)_{nf}$ and κ_{nf} denote, respectively, the effective density, dynamic viscosity, electrical conductivity, heat capacity and thermal conductivity of the nanofluid.

INTERNATIONAL JOURNAL OF EXPLORING EMERGING TRENDS IN ENGINEERING
Peer-Reviewed, Refereed, Indexed and International Journal, https://ijoeete.com/
(Peer Review Journal as per UGC 2025 Standard Guidelines)
|ISSN No. 2394-0573 |Volume: 13, Issue: 2 | April – June 2026

The effective nanofluid properties are evaluated from the classical mixture relations of Prasad and Jaychandra[12,13]:

$$\mu_{nf} = \frac{\mu_f}{(1-\phi)^{2.5}} \tag{4}$$

$$\rho_{nf} = (1-\phi)\rho_f + \phi\rho_s \tag{5}$$

$$\sigma_{nf} = (1-\phi)\sigma_f + \phi\sigma_s \tag{6}$$

$$(\rho C_p)_{nf} = (1-\phi)(\rho C_p)_f + \phi(\rho C_p)_s \tag{7}$$

$$\frac{k_{nf}}{k_f} = \frac{k_s + 2k_f - 2\phi(k_f - k_s)}{k_s + 2k_f + \phi(k_f - k_s)} \tag{8}$$

The subscripts *nf*, *f* and *s* refer to the nanofluid, base fluid and solid nanoparticles, respectively; ϕ is the solid volume fraction.

The appropriate boundary conditions that incorporate the melting effect at the solid–liquid interface are

$$\begin{aligned}
&u\left(x, A(x+b)^{\frac{1-m}{2}}\right) = U_w(x) = U_0(x+b)^m \\
&\kappa_{nf}\left(\frac{\partial T}{\partial y}\right)_{y=A(x+b)^{\frac{1-m}{2}}} = \rho_{nf}\left[\lambda + C_s(T_m - T_0)\right]v\left(x, y = A(x+b)^{\frac{1-m}{2}}\right) \\
&T\left(x, A(x+b)^{\frac{1-m}{2}}\right) = T_m \\
&u(x,\infty) = 0, \quad T(x,\infty) = T_\infty
\end{aligned} \tag{9}$$

where λ is the latent heat of fusion and C_s is the specific heat of the solid phase.

Introduction of the similarity variables

$$\psi = \eta f(\eta)\sqrt{\frac{2}{m+1}\nu_f U_0(x+b)^{m+1}}, \eta = y\sqrt{\frac{m+1}{2}\cdot\frac{U_0(x+b)^{m-1}}{\nu_f}}, \theta(\eta) = \frac{T-T_m}{T_\infty - T_m} \tag{10}$$

together with the stream-function definition $u = \partial\psi/\partial y$, $v = -\partial\psi/\partial x$ yields the velocity components

$$u = \frac{\partial\psi}{\partial y} = U_0(x+b)^m f'(\eta), v = -\frac{\partial\psi}{\partial x} = -\sqrt{\frac{m+1}{2}\nu_f U_0(x+b)^{m-1}}\left[f'(\eta)\cdot\eta\frac{m-1}{m+1} + f(\eta)\right] \tag{11}$$

Substitution of the similarity variables into the momentum and energy equations produces the following system of ordinary differential equations:

$$f''' + (1-\phi)^{2.5}\left\{1-\phi+\phi\frac{\rho_s}{\rho_f}\right\}\left(ff'' - \frac{2m}{m+1}f'^2\right) - M^2(1-\phi)^{2.5}\left(1-\phi+\phi\frac{\sigma_s}{\sigma_f}\right)f' = 0 \tag{12}$$

$$\frac{1}{\Pr}\frac{\kappa_{nf}}{\kappa_f}\theta'' + \left\{1-\phi+\phi\frac{(\rho C_p)_s}{(\rho C_p)_f}\right\}\left(f\theta' - \frac{1-m}{1+m}f'\theta\right) = 0 \tag{13}$$

INTERNATIONAL JOURNAL OF EXPLORING EMERGING TRENDS IN ENGINEERING
Peer-Reviewed, Refereed, Indexed and International Journal, https://ijoeete.com/
(Peer Review Journal as per UGC 2025 Standard Guidelines)
|ISSN No. 2394-0573 |Volume: 13, Issue: 2 | April – June 2026

in which M is the magnetic-field parameter and Pr is the Prandtl number. The associated boundary conditions become

$$f'(\delta)=1,\quad \frac{\kappa_{nf}}{\kappa_f}Me\cdot\theta'(\delta)+\left\{1-\phi+\phi\frac{\rho_s}{\rho_f}\right\}\Pr\left[f(\delta)+\frac{m-1}{m+1}\delta\right]=0$$
$$\theta(\delta)=0,\quad f'(\infty)=0,\quad \theta(\infty)=1 \tag{14}$$

Here δ is the wall-thickness parameter and Me is the melting parameter. For computational convenience the domain $[\delta, \infty)$ is shifted to $[0, \infty)$ by the translation $\xi = \eta - \delta$, $F(\xi) = f(\eta)$, $\Theta(\xi) = \theta(\eta)$, resulting in the final boundary-value problem

$$F'''+(1-\phi)^{2.5}\left\{1-\phi+\phi\frac{\rho_s}{\rho_f}\right\}\left(FF''-\frac{2m}{m+1}F'^2\right)-M^2(1-\phi)^{2.5}\left(1-\phi+\phi\frac{\sigma_s}{\sigma_f}\right)F'=0 \tag{15}$$

$$\frac{1}{\Pr}\frac{\kappa_{nf}}{\kappa_f}\Theta''+\left\{1-\phi+\phi\frac{(\rho C_p)_s}{(\rho C_p)_f}\right\}\left(F\Theta'-\frac{1-m}{1+m}F'\Theta\right)=0 \tag{16}$$

The corresponding boundary conditions restructured as

$$F'(0)=1,\quad \frac{\kappa_{nf}}{\kappa_f}Me\cdot\Theta'(0)+\left\{1-\phi+\phi\frac{\rho_s}{\rho_f}\right\}\Pr\left[F(0)+\frac{m-1}{m+1}\delta\right]=0$$
$$\Theta(0)=0,\quad F'(\infty)=0,\quad \Theta(\infty)=1 \tag{17}$$

Quantities of engineering interest are the local skin-friction coefficient and the local Nusselt number,

$$C_f=\frac{2\mu_{nf}}{\rho_{nf}u_w^2}\left(\frac{\partial u}{\partial y}\right)_{y=A(x+b)^{\frac{1-m}{2}}}=\frac{\sqrt{2(m+1)}\,F''(0)}{\left[(1-\phi)+\phi\frac{\rho_s}{\rho_f}\right](1-\phi)^{2.5}}\mathrm{Re}_x^{-\frac{1}{2}} \tag{18}$$

$$Nu=-\frac{(x+b)\kappa_{nf}}{\kappa_f(T_\infty-T_m)}\left(\frac{\partial T}{\partial y}\right)_{y=A(x+b)^{\frac{1-m}{2}}}=-\sqrt{\frac{m+1}{2}}\frac{\kappa_{nf}}{\kappa_f}\mathrm{Re}_x^{\frac{1}{2}}\Theta'(0) \tag{19}$$

Where, $Re_x = U_0(x+b) / \nu_f$ denotes the local Reynolds number.

Thus we from Eqs. (18) and (19) have

$$C_{fr}=\mathrm{Re}_x^{\frac{1}{2}}C_f=\frac{\sqrt{2(m+1)}\,F''(0)}{\left[(1-\phi)+\phi\frac{\rho_s}{\rho_f}\right](1-\phi)^{2.5}} \tag{20}$$

$$Nu_r=Nu\cdot\mathrm{Re}_x^{-\frac{1}{2}}=-\sqrt{\frac{m+1}{2}}\frac{\kappa_{nf}}{\kappa_f}\Theta'(0) \tag{21}$$

Table 1 — Thermophysical characteristics of base liquid and nanoparticle

INTERNATIONAL JOURNAL OF EXPLORING EMERGING TRENDS IN ENGINEERING
Peer-Reviewed, Refereed, Indexed and International Journal, https://ijoeete.com/
(Peer Review Journal as per UGC 2025 Standard Guidelines)
|ISSN No. 2394-0573 |Volume: 13, Issue: 2 | April – June 2026

Physical characteristics	Water	Silver
Specific heat capacity	4.179	235
Density	997.1	10500
Thermal conductivity	0.613	429
Electrical conductivity	5.5×10^6	3.5×10^7

Results and Discussion

Numerical solutions are obtained for a range of governing parameters. Unless otherwise stated, the fixed values used are Pr = 6.2, $\delta = 0.25$, m = 1.0, $\phi = 0.02$, M = 1.0 and Me = 0 or 2, while the parameter under examination is allowed to vary.

An increase in the wall-thickness parameter δ lowers the velocity throughout the boundary layer for both melting and non-melting cases (Fig. 2a). A larger value of δ corresponds to a slower variation of surface velocity, which reduces the shear that drives the flow. The temperature profiles also decrease with rising δ (Fig. 2b), indicating a thinner thermal boundary layer.

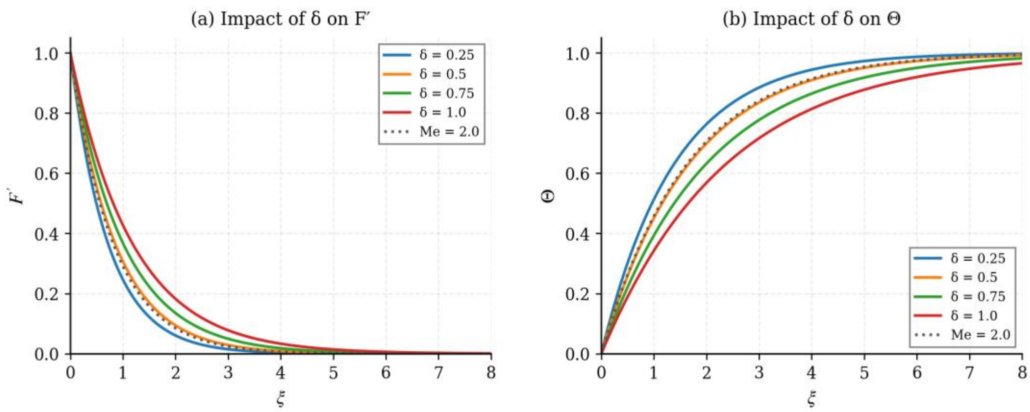

Fig. 2 — Impact of (a) δ on F′, and (b) δ on Θ

Raising the power-law index m increases the velocity (Fig. 3a) while decreasing the temperature (Fig. 3b).Higher values of m strengthen the stretching rate near the leading edge, accelerating the fluid and shortening the time available for heat diffusion.

INTERNATIONAL JOURNAL OF EXPLORING EMERGING TRENDS IN ENGINEERING
Peer-Reviewed, Refereed, Indexed and International Journal, https://ijoeete.com/
(Peer Review Journal as per UGC 2025 Standard Guidelines)
|ISSN No. 2394-0573 |Volume: 13, Issue: 2 | April – June 2026

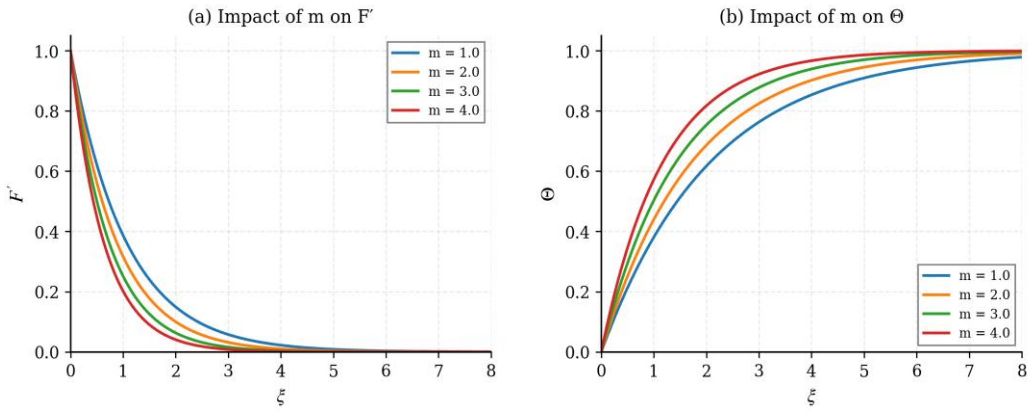

Fig. 3 — Impact of (a) m on F′, and (b) m on Θ

A stronger magnetic field (larger M) decelerates the flow (Fig. 4a). The Lorentz force acts as a resistive body force, opposing the motion and thickening the momentum boundary layer. Under melting conditions the temperature also falls modestly with increasing M (Fig. 4b).

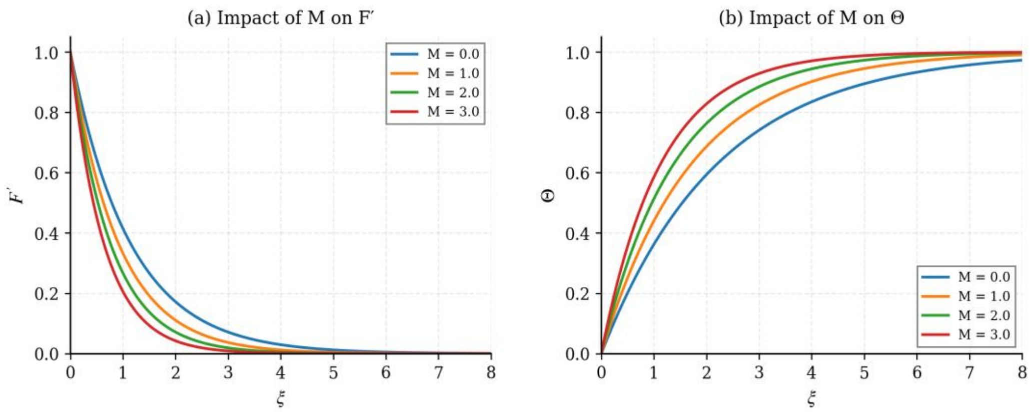

Fig. 4 — Impact of (a) M on F′, and (b) M on Θ

Increasing the melting parameter Me reduces both velocity and temperature (Fig. 5). Melting absorbs latent heat at the solid–liquid interface, cooling the neighbouring fluid and weakening the thermal driving force. As a result, both skin friction and wall heat-transfer rate decrease with rising Me(Table 5).

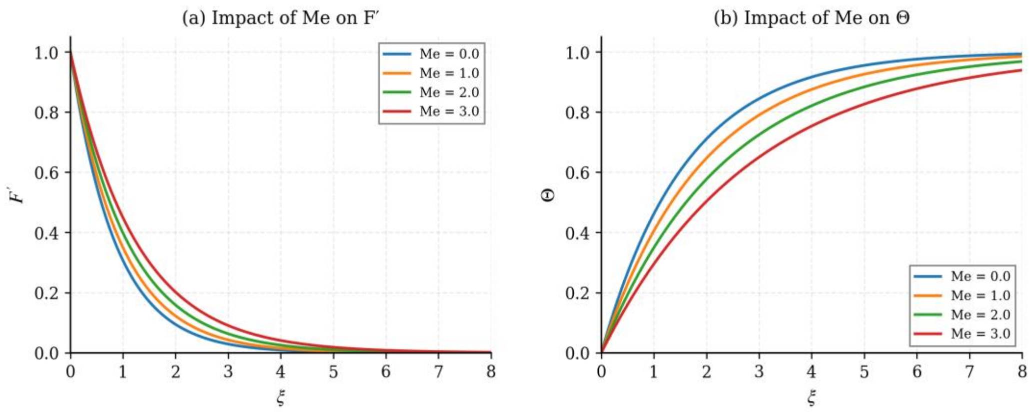

INTERNATIONAL JOURNAL OF EXPLORING EMERGING TRENDS IN ENGINEERING
Peer-Reviewed, Refereed, Indexed and International Journal, https://ijoeete.com/
(Peer Review Journal as per UGC 2025 Standard Guidelines)
|ISSN No. 2394-0573 |Volume: 13, Issue: 2 | April – June 2026

Fig. 5 — Impact of (a) Me on F′, and (b) Me on Θ

Higher nanoparticle volume fraction ϕ increases the effective viscosity and therefore retards the velocity (Fig. 6a). At the same time the enhanced thermal conductivity of the nanofluid steepens the near-wall temperature gradient, reducing the thickness of the thermal boundary layer (Fig. 6b).

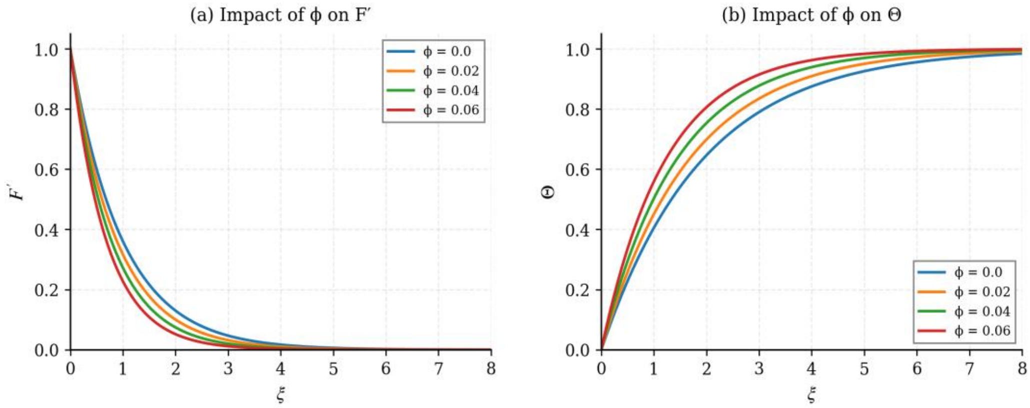

Fig. 6 — Impact of (a) ϕ on F′, and (b) ϕ on Θ

Validation of the present numerical scheme is provided in Table 2, where values of −F″(0) for the Ag–water nanofluid are compared with the benchmark results of Hamad[28] and Acharya et al.[10]. The excellent agreement confirms the reliability of the computational procedure. Tables 3 and 4 summarise the quantitative influence of δ, m, M and ϕ on the reduced skin-friction coefficient C_{fr} and the reduced Nusselt number Nu_r for the two melting rates $Me = 0$ and $Me = 2$.

Table 2 — Comparison of the values of −F″(0) for Ag-H_2O for different values of M, ϕ

M	ϕ	Hamad[28]	Acharya et al.[10]	Present work
0.0	0.05	1.13966	1.139648	1.139648
—	0.1	1.22507	1.225041	1.225041
—	0.15	1.27215	1.272106	1.272106
—	0.2	1.28979	1.289711	1.289711
0.5	0.05	1.31858	1.318527	1.318527
—	0.1	1.37296	1.372951	1.372951
—	0.15	1.39694	1.396978	1.396978
—	0.2	1.39634	1.396320	1.396320

INTERNATIONAL JOURNAL OF EXPLORING EMERGING TRENDS IN ENGINEERING
Peer-Reviewed, Refereed, Indexed and International Journal, https://ijoeete.com/
(Peer Review Journal as per UGC 2025 Standard Guidelines)
|ISSN No. 2394-0573 |Volume: 13, Issue: 2 | April – June 2026

Table 3 — Impact of flow variables on C_{fr}

Note: When a parameter is varied, the remaining parameters are kept fixed.

δ	m	M	ϕ	Me = 0.0	Me = 2.0
Effect of δ (m = 2.0, M = 1.0, ϕ = 0.02)					
0.25	2.0	1.0	0.02	-2.050500	-2.063899
0.50	2.0	1.0	0.02	-1.765503	-1.783721
0.75	2.0	1.0	0.02	-1.531278	-1.552039
1.00	2.0	1.0	0.02	-1.340707	-1.362194
Effect of m (δ = 0.25, M = 1.0, ϕ = 0.02)					
0.25	1.0	1.0	0.02	-1.385022	-0.900551
0.25	2.0	1.0	0.02	-1.829544	-1.428042
0.25	3.0	1.0	0.02	-2.191721	-1.834722
0.25	4.0	1.0	0.02	-2.515433	-2.047015
Effect of m (δ = 2.0)					
2.0	0.0	—	—	-1.792140	-1.779813
2.0	1.0	—	—	-2.005027	-1.951781
2.0	2.0	—	—	-2.145940	-2.109987
2.0	3.0	—	—	-2.680642	-2.448157
Effect of ϕ					
—	—	—	0.00	-2.752849	-2.585165
—	—	—	0.02	-2.525527	-2.341564
—	—	—	0.04	-2.209815	-2.009187
—	—	—	0.06	-1.988851	-1.778689

Table 4 — Impact of flow variables on Nu_r

Note: When a parameter is varied, the remaining parameters are kept fixed.

δ	m	M	ϕ	Me = 0.0	Me = 2.0
Effect of δ (m = 2.0, M = 1.0, ϕ = 0.02)					
0.25	2.0	1.0	0.02	-0.633175	-0.572103
0.50	2.0	1.0	0.02	-0.524288	-0.470647
0.75	2.0	1.0	0.02	-0.423695	-0.378754
1.00	2.0	1.0	0.02	-0.331979	-0.295699
Effect of m (δ = 0.25, M = 1.0, ϕ = 0.02)					
0.25	1.0	1.0	0.02	-0.445163	-0.413168
0.25	2.0	1.0	0.02	-0.421106	-0.390605

0.25	3.0	1.0	0.02	-0.397761	-0.370235
0.25	4.0	1.0	0.02	-0.350160	-0.326175
Effect of m ($\delta = 2.0$)					
2.0	0.0	—	—	-0.498166	-0.343006
2.0	1.0	—	—	-0.453926	-0.325504
2.0	2.0	—	—	-0.430875	-0.294503
2.0	3.0	—	—	-0.379940	-0.257203
Effect of ϕ					
—	—	—	0.00	-0.744093	-0.744093
—	—	—	0.02	-0.625443	-0.561314
—	—	—	0.04	-0.591536	-0.504785
—	—	—	0.06	-0.561089	-0.438387

Table 5 — Impact of melting variable on Cf_r and Nu_r

Me	Cf_r	Nu_r
0.0	-1.837001	-0.666117
1.0	-1.615995	-0.458378
2.0	-1.492526	-0.357507
3.0	-1.407518	-0.296000

Conclusion

A numerical study of MHD flow and heat transfer of an Ag–water nanofluid over a stretching sheet of variable thickness in the presence of melting has been carried out. The main findings are summarised below.

(i) Increasing the wall-thickness parameter δ reduces both velocity and temperature inside the boundary layer and raises the magnitudes of skin friction and Nusselt number.

(ii) Larger values of the power-law index m accelerate the flow, cool the fluid and increase wall shear stress and heat-transfer rates.

(iii) A stronger magnetic field retards the motion and modestly lowers the temperature under melting conditions.

(iv) The melting parameter Me decreases both velocity and temperature and reduces the absolute values of skin friction and Nusselt number relative to the non-melting case.

(v) Higher nanoparticle volume fraction ϕ slows the flow while improving the near-wall temperature gradient and heat-transfer rate.

The numerical results have been validated against existing benchmark data. The findings offer useful guidance for the design of thermal systems that involve melting and variable-geometry stretching surfaces.

References

1. Jayachandra Babu M, Sandeep N & Nuhat A O, Magnetohydrodynamic dissipative flow across the linearly stretching sheet with temperature-dependent variable viscosity, *Results Phys*, 7 (2017) 1801–1807.
2. Hayat T, Qayyum S, Imtiaz M & Alsaedi A, Radiative flow due to stretchable rotating disk with variable thickness, *Results Phys*, 7 (2017) 156–165.
3. Asghar S A, Steady Boundary Layer Magnetohydrodynamic Viscous Flow and Heat Transfer of Nanofluid Over Stretching Sheet in Presence of Radiation and Heat Source, *J Nanofluids*, 6 (2017) 1206–1214.
4. Kumar R, Kiran M S S, Varma S V K, Hydromagnetic power-law fluid slip flow of nanofluid through porous medium over a slendering stretching sheet, *J Nanofluids*, 6 (2017) 881–889.
5. Mabood F & Das K, Melting heat transfer on hydromagnetic flow of a nanofluid over a stretching sheet with radiation and second-order slip, *Int J Heat Mass Tran*, 131 (2016) 3.
6. Prasanna Kumara B C, Ramesh G K, Chamkha A J & Gireesha B J, Stagnation-point flow of a viscous fluid towards a stretching surface with variable thickness and thermal radiation, *Int J Industrial Mathematics*, Article ID IJM-00685.
7. Fang T, Zhang J & Zhong Y, Boundary layer flow over a stretching sheet with variable thickness, *Appl Math Comput*, 218 (2012) 7241–7252.
8. Elbashbeshy E M A, Emam T G & Abdel-wahed M S, Flow and heat transfer over a moving surface with nonlinear velocity and variable thickness in a nanofluid in the presence of thermal radiation, *Can J Phys*, 92 (2014) 124–130.
9. Abdel-wahed M S, Elbashbeshy E M A & Emam T G, Flow and heat transfer over a moving surface having different types of velocity and variable thickness in nanofluids in the presence of Brownian motion, *Appl Math Comput*, 254 (2015) 49–62.
10. Acharya N, Das K & Kundu P K, Ramification of variable thickness on MHD TiO_2 and Ag nanofluid flow over a stretching sheet using NDSolve, *Eur Phys J Plus*, 131 (2016) 303–312.
11. Khan M, Azam M & Alshomrani A S, Effects of melting and heat generation/absorption on unsteady Falkner-Skan flow of Carreau nanofluid over a wedge, *Int J Heat Mass Tran*, 110 (2017) 437–446.
12. Prasad K V, Vajravelu K, Vaidya H & Van Gorder R A, MHD flow and heat transfer in a nanofluid over a slendering elastic sheet with variable thickness, *Results Phys*, 7 (2017) 1462–1474.
13. Jayachandra Babu M & Sandeep N, MHD Non-Newtonian fluid flow over a slendering stretching sheet in the presence of cross-diffusion effects, *Alex Eng J*, 55 (2016) 2193–2201.
14. Hayat T, Muhammad K, Farooq M, Alsaedi A, Melting heat transfer in stagnation point flow of carbon nanotubes towards variable thickness surface, *Adv Adv*, 6 (2016) 015124.
15. Gireesha B J, Mahanthesh B, Shivakumara I S & Eshwarappa K M, Melting heat transfer in boundary layer stagnation-point flow of nanofluid toward a stretching sheet with induced magnetic field, *Eng Sci Tech Int J*, 19 (2016) 313–321.
16. Hayat T, Ullah I, Alsaedi A & Farooq M, MHD flow of Powell-Eyring nanofluid over a non-linear stretching sheet with variable thickness, *Results Phys*, 7 (2017) 189–196.
17. Qayyum S, Hayat T, Alsaedi A, Magnetohydrodynamic (MHD) nonlinear convective flow of Walters-B nanofluid over a nonlinearly stretching sheet with variable thickness, *Int J Heat Mass Tran*, 110 (2017) 506–514.
18. Anjali Devi S P & Prakash M, Slip flow effects over hydromagnetic forced convective flow over a slendering stretching sheet, *J Appl Fluid Mech*, 9 (2016) 683–692.
19. Anjali Devi S P & Prakash M, Temperature dependent viscosity and thermal conductivity effects on

hydromagnetic flow over a slendering stretching sheet, *J Niger Math Soc*, 34 (2015) 318–330.

20. Anjali Devi S P & Prakash M, Thermal radiation effects on hydromagnetic flow over a slendering stretching surface, *J Braz Soc Mech Sci Eng*, 38 (2016) 423–431.

21. Nadeem N, Tahir B, Labropulu F & Akbar N S, Unsteady axisymmetric stagnation point flow of a Jeffrey fluid, *J Aerosp Eng*, 27 (2014) 636–643.

22. Nadeem S, Rashid M & Sher A N, Optimized analytical solution for oblique flow of a Casson-nano fluid with convective boundary conditions, *Int J Therm Sci*, 78 (2014) 90–100.

23. Parida S, Mehmood R & Akbar N S, Partial slip effects on non-aligned stagnation point nanofluid over a stretching convective surface, *Chin Phys B*, 24 (1) (2015) 014702.

24. Parida S K & Mishra S R, Heat and mass transfer of MHD nanofluid flow over a stretching sheet in nanofluid in the presence of thermal radiation, *J Nanofluids*, 8 (1) (2018) 143–149.

25. Mishra S R & Rout B C, Analytical solution of electrically conducting water-based (KKL model) nanofluid flow over a linearly stretching sheet, *Iran J Sci Technol Trans Mech Eng*.

26. Wakit A, Boualhy Z, Mishra S R, Rashidi M M, Sohag R, The free convection of a nanofluid in an inclined cavity: the thermo-hydrodynamic stability in water-based nanofluid with metallic nanoparticles using a generalized Buongiorno's mathematical model, *Eur Phys J Plus*, 133 (2018) 1–18.

27. Rout B C & Mishra S R, Thermal energy transport in nanofluid flow of non-Newtonian fluid: A comparative study, *JAMECH*, 21 (1) (2018) 60–69.

28. Hamad M A A, Analytical solution of natural convection flow of a nanofluid over a linearly stretching sheet in the presence of magnetic field, *Int Commun Heat Mass Tran*, 38 (2011) 487–492.